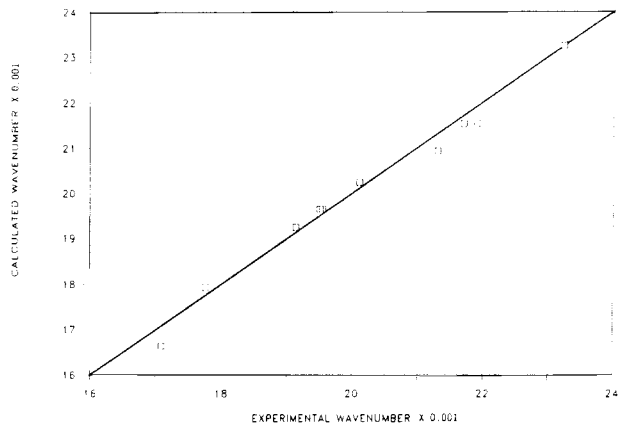

Figure 5. Empirical correlation of S_1 state energies in substituted anthraquinones. Theoretical line of unit slope is drawn. The best linear fit to the data has a slope of 0.982 and a correlation coeficient of 0.992. From upper right to lower left the points correspond to AQ, 1-HAQ, 1,8-DHAQ, 1,5-DHAQ, 1-AAQ, 1,5-DAAQ, 1-A-5-HAQ, 1,4-DHAQ, 1-A-4-HAQ, and 1,4-DAAQ.

analysis too hard. From the separation of the zeroth-order states (ca. 600 cm^{-1}) and the energy shifts of 500 and 800 cm^{-1}, we *very roughly* estimate the coupling matrix element V to be on the order of 500 cm^{-1}.

We have attempted similar analyses of the spectra for 1,5-DAAQ and 1,5-DHAQ. In each of these cases the zeroth-order states are identical and the observed spectrum is primarily a shifted version of the spectrum of the corresponding monosubstituted anthraquinone but with differences in the overall band shape between the mono- and disubstituted forms, especially for the 1-HAQ and 1,5-DHAQ (Figure 4). There is no obvious evidence for a second excited state on the tail of the S_1 absorbance. Note that the simple two-state perturbation analysis would predict exact cancellation of transition moments to the minus (higher energy) combination of zeroth-order states. The additional shift brought about by the second substituent in the 5-position is 600 cm^{-1} for 1,5-DAAQ and 725 cm^{-1} for 1,5-DHAQ.

The entire data set is accommodated by the energy gap correlation shown in Figure 5, where we have plotted the experimental S_1 state energies along the abscissa and a calculated energy on the ordinate. The calculated energy is in the form

$$23300 - 3000N_A - 1700N_H - 600I$$

where N_A and N_H are the number of amino and hydroxy groups, respectively, in the 1- and 4-positions, and I is a disubstitution interaction parameter equal to 1 for the 1,4- and 1,5-forms and 0 for the 1,8- and monosubstituted molecules; in the mixed molecule 1-A-5-HAQ we take $N_A = 1$, $N_H = 0$, and $I = 1$ since the S_1 state is amino-like. For such a simple model the correlation is impressively linear ($R^2 = 0.984$; slope = 0.986).

The energy gap correlation is useful for the consideration of excited-state proton-transfer processes in these and similar molecules, but it would be even more useful if a similar correlation were available for the 1,10-quinone excited-state energies. The position of the lower energy 1,10-quinone forms in S_1 is known for 1-HAQ (20 730 cm^{-1}), 1,5-DHAQ (20 250 cm^{-1}), and 1,8-DHAQ (21 121 cm^{-1}), but for none of the other molecules in the data set.

We have used Shpolskii matrix data in the correlation. The objection might be raised that the correlation is compromised since the matrix stabilization will be different depending on the relative excited- and ground-state dipole moments of the various molecules. However, gas-phase data can be shown to not significantly affect the correlation. Matrix-to-gas-phase shifts for 1-HAQ, 1,4-DHAQ, 1,5-DHAQ, 1,8-DHAQ, and 1-AAQ are 20, 21, 23, 20, and 25 nm, respectively.

Conclusions

The S_1 electronic state energies of substituted anthraquinones follow a predictable pattern as a function of type of substituent and position of substitution. An $-NH_2$ group has a greater effect on the S_1 energy than does an $-OH$ group. There is a strong interaction between substituents para to each other on the same outer anthraquinone ring, whereas 1,5-substituents interact only a little. The suggestion that anthraquinone can be viewed as two "half-molecules" with the division along a diagonal line has been confirmed and strengthened. The experimental absorbance spectrum of 1-amino-5-hydroxyanthraquinone is well accounted for by summing the individual 1-aminoanthraquinone and 1-hydroxyanthraquinone spectra.

Acknowledgment. This work was supported by grants from the National Science Foundation (CHE-8111960 and CHE-8608629). We also thank the Hewlett-Packard Corp., which provided the diode array spectrophotometer used for the room-temperature solution spectra.

Registry No. AQ, 84-65-1; 1-HAQ, 129-43-1; 1,8-DHAQ, 117-10-2; 1,5-DHAQ, 117-12-4; 1-AAQ, 82-45-1; 1,4-DHAQ, 81-64-1; 1-A-5-HAQ, 71502-46-0; 1,5-DAAQ, 129-44-2; 1-A-4-HAQ, 116-85-8; 1,4-DHAQ, 128-95-0.

Vibration-Induced Electron Detachment in Acetaldehyde Enolate Anion

Douglas O'Neal and Jack Simons*

Department of Chemistry, University of Utah, Salt Lake City, Utah 84112 *(Received: February 29, 1988)*

Fully ab initio theoretical simulations of the rates of electron detachment caused by the non-Born–Oppenheimer coupling of vibrational and electronic states in the acetaldehyde enolate anion have been performed. The state-specific rates of electron ejection are discussed, and an RRKM model is used to simulate the rate of electron loss for anions that have been activated by sequential infrared photon absorption. The relationship to experimental data on acetone enolate is discussed, and it is shown that the observed rates of electron loss are consistent with the proposed mechanism.

Introduction

Ion cyclotron resonance (ICR) experiments[1] of the Brauman and Beauchamp groups showed that vibrationally excited molecular anions can undergo electron detachment. Previous theoretical calculations by Acharya et al.[2] indicate that, in cases for which the anion and neutral molecule electronic energy surfaces do *not* intersect, such detachments may be interpreted by using

(1) Meyer, F. K.; Jasinski, J. M.; Rosenfeld, R. N.; Brauman, J. I. *J. Am. Chem. Soc.* **1982**, *104*, 663. Rosenfeld, R. N.; Jasinski, J. M.; Brauman, J. I. *J. Chem. Phys.* **1979**, *71*, 1030. Wight, C. A.; Beauchamp, J. L. *J. Am. Chem. Soc.* **1981**, *103*, 6501.

(2) (a) Acharya, P. K.; Kendall, R. K.; Simons, J. *J. Am. Chem. Soc.* **1984**, *106*, 3402; *J. Chem. Phys.* **1985**, *83*, 3888. (b) Chalasinski, G.; Kendall, R. A.; Taylor, H. L.; Simons, J. *J. Phys. Chem.* **1988**, *92*, 3086. (c) Simons, J. *J. Am. Chem. Soc.* **1981**, *103*, 3971. (d) Neumark, D. M.; Lykke, K. R.; Andersen, T.; Lineberger, W. C. *J. Chem. Phys.* **1985**, *83*, 4364.

0022-3654/89/2093-0058$01.50/0

a second-order Fermi Golden Rule framework in which the perturbation is the dynamic coupling between the vibrational and electronic degrees of freedom. The work of Acharya et al. examined two diatomic species, LiH^- and OH^-, that were viewed, respectively, as fast and slow limiting cases for the rate of vibration-induced electron detachment (VIED). State-specific rates of electron ejection were predicted to range from 10^5 to 10^{10} s^{-1} for LiH^- and 10^2 to 10^6 s^{-1} for OH^-. Subsequently, the propensities for state-specific electron ejection for rotationally assisted processes have been treated by us[2b] and applied to the experimentally[2d] studied NH^- species. The current work involves a much larger system with many internal degrees of freedom, the acetaldehyde enolate anion $^-CH_2$–CH=O, and one whose rates of electron loss can be compared to experimental work on a similar species.

It is useful to review certain features of the experimental procedure to clarify the meaning of our ab initio results. The Brauman group[1,3] used a pulsed infrared ($\lambda^{-1} \sim 1047$ cm^{-1}) laser with a fluence of 0.1–6 J/cm^2 to excite the anions in an ICR cell. The pressure in the cell is thought to be $\sim 10^{-6}$ Torr, so essentially collisionless conditions prevail during the laser pulse duration of 1000 ns. The laser pulse is characterized by an intense pulse lasting ~ 100 ns, which contains approximately 50% of the energy, followed by a weaker long "tail" lasting ~ 1000 ns, which contains the remaining 50% of the energy. The adiabatic detachment energies (DE) of the anions that were studied are great enough (>0.3 eV) that several infrared photons must be absorbed for electron ejection to be energetically possible. For the enolates, whose DE's generally lie near 1.8 eV, Beer–Lambert plots of the ICR signal with and without the laser turned on are used to phenomenologically extract IR absorbance cross sections (σ) which generally range from 10^{-21} to 10^{-19} cm^2.

These cross sections (specifically $\sigma = 10^{-19}$ cm^2 for $H_3CCOCH_2^-$), combined with the parameters of the laser source, give rise to a picture in which IR photons are sequentially absorbed by the anion once every $\sim 10^{-7}$ s. In the Brauman experiments,[3] the acetone enolate anions absorb IR photons at this rate until they have enough internal energy to either eject an electron or undergo unimolecular decomposition to give methane and deprotonated ketene $CH_4 + HCCO^-$. The energy thresholds for the ejection and dissociation paths are approximately 14 000 and 21 000 cm^{-1}, respectively for acetone enolate. Because both decay channels were observed, they must occur at comparable rates under the experimental conditions. Using the known threshold for the unimolecular decay channel and making an RRKM estimate of its decay rate, Brauman et. al. estimated that the dissociation rate would equal the "up pumping" rate of 10^7 s^{-1} at approximately 1000 cm^{-1} above the dissociation threshold or 8000 cm^{-1} above the electron ejection threshold. This, of course, then implies that electron ejection is occurring at a rate of $\sim 10^7$ s^{-1} when the ion has internal energy that exceeds the detachment threshold by 8000 cm^{-1}.

In this paper we present our theoretical simulation of the electron ejection process for the $HCOCH_2^-$ enolate and attempt to compare, within a reasonable model, our results with the available experimental data. Our results indicate that non-Born–Oppenheimer coupling can explain the electron ejection process for these enolate systems. We do not know for certain that the enolate and the corresponding neutral radical electronic energy surfaces do not cross as the anion vibrates. However, we can say that the excellent agreement between our computed rates and those experimentally observed gives no evidence that such crossings (at which rates of ejection would be *very* fast $\sim 10^{14}$ s^{-1}) occur.

In earlier papers,[2] we derived expressions for the rate of electron ejection from vibrationally or rotationally (V/R) excited anions *assuming* that nonadiabatic coupling provides the mechanism for V/R to electronic energy flow. For all of the systems studied theoretically by our group, the electronic energy of the anion lies below that of the neutral for most or all of the range of the anion's vibrational coordinate. Thus, if only electronic processes (and energy) were involved (i.e., if the motion of the nuclei were decoupled), it would be energetically impossible for the anion to lose an electron spontaneously. It is only as the anion vibrates that the *total* energy of the anion exceeds that of the radical (in a lower vibrational state). Once the combined electronic-plus-vibration/rotation energy is considered, it is possible to postulate a mechanism that couples the electronic and vibrational degrees of freedom, thereby ejecting an electron.

For the enolates being considered here, it is thought that those vibrations that most strongly modulate the orbital in which the "active" electron resides play the central role in this coupling. Within this assumption, it is possible to ignore overall rotation of the enolate and to ultimately treat all but these "important" vibrations in a passive manner as described below. We label the electronic states of the anion and the neutral-plus-free electron as Ψ^- and Ψ_k^0, respectively, and the corresponding vibrational states as χ_ν^- and χ_ν^0. The matrix element that couples these states was shown in ref 3 to be of the form

$$V_{if} = -(\hbar^2/2\mu) \int\int (\chi_\nu^0 \Psi_k^0)^* [2\nabla_{\tilde{Q}} \chi_\nu^- \cdot \nabla_{\tilde{Q}} \Psi^- + \chi_\nu^- \nabla_{\tilde{Q}}^2 \Psi^-] \, d\vec{r} \, d\tilde{Q} \quad (1)$$

where μ is a reduced mass, $\tilde{Q}$ denotes the set of $3N-6$ vibrational coordinates, and $\vec{r}$ denotes the coordinates of all of the electrons. The nuclear kinetic energy operator $-(\hbar^2/2\mu)\nabla_{\tilde{Q}}^2$ operating on the electronic wave function $\Psi^-(\vec{r}|\tilde{Q})$ will give a result proportional to m_e/μ times the electronic kinetic energy operator acting on the same wave function. Thus, the second term in eq 1 is expected to be smaller than the first term by a factor of $(m_e/\mu)^{1/2}$, as a result of which we can drop this second term. The state-to-state transition rate from the anion to the neutral is then given by

$$W = (2\pi/\hbar)|V_{if}|^2\rho = (2\pi\hbar^3/\mu^2) \times \left|\int\int (\chi_\nu^0(Q)\Psi_k^0(\mathbf{r}|Q))^* \nabla_Q \chi_\nu(Q) \nabla_Q \Psi^-(\mathbf{r}|Q) \, d\mathbf{r} \, dQ\right|^2 \rho \quad (2)$$

where ρ is the density of translational states of the free electron in a (large) box of side L and energy $\hbar^2k^2/(2m_e)$:

$$\rho = \frac{m_e L^3 k}{2\pi^2 \hbar^2} \quad (3)$$

The electronic wave functions of the anion and neutral are treated, in this work, at the single Slater-determinant level. Moreover, all of the occupied molecular orbitals of the two species are assumed to be identical except for the highest occupied orbital ϕ_- (HOMO) of the anion which corresponds to the free-electron orbital ϕ_k of Ψ_k^0. This level of treatment ignores all electron correlation effects and assumes that relaxation of the "inactive" orbitals of the neutral is negligible. Clearly, these are approximations, and the resulting simulations therefore represent the simplest reasonable treatment of the electron ejection process. This level of treatment served us well in our earlier studies[2] and seems to be appropriate here, although, as discussed below, it is necessary, as a result, to shift the anion and neutral potential energy curves relative to one another to correctly reproduce the detachment threshold.

In the present work, the orbital ϕ_k is described by a plane wave orbital having kinetic energy $\hbar^2k^2/2m_e$ and constructed to be orthogonal to the occupied "inactive" orbitals. With all of these simplifications, the Slater–Condon rules reduce the rate expression in eq 2 to an expression involving only the active orbitals:

$$W = (2\pi\hbar^3/\mu^2)\left|\int \chi_\nu^0(Q) \int \phi_k^*(\mathbf{r}|Q) \nabla_Q \phi_-(\mathbf{r}|Q) \, d\mathbf{r} \, \nabla_Q \chi(Q) \, dQ\right|^2 \rho \quad (4)$$

This is our final working equation.

The active orbital in acetaldehyde enolate anion is the "nonbonding" 2π orbital, which is a superposition of 2p orbitals on the terminal carbon and oxygen atoms with small amplitude on the central carbon. One mode of vibration that greatly affects

(3) Foster, R. F.; Tumas, W.; Brauman, J. I. *J. Chem. Phys.* **1983**, *79*, 4644; also see the following paper in this issue.

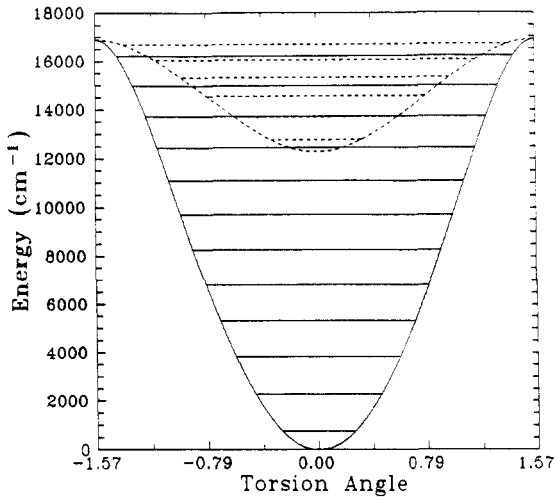

Figure 1. Born–Oppenheimer energy curves and vibrational energy levels for acetaldehyde enolate anion (solid line) and neutral (dashed line).

TABLE I: Optimized Equilibrium Geometry of CH_2COH^-

C–C′ bond dist, Å	1.35	O–C–C′ bond angle, deg	111.1
C–O bond dist, Å	1.46	H–C–C′ bond angle, deg	135.8
C–H bond dist, Å	1.24	C–C′–H′ bond angle, deg	119.0
C′–H′ bond dist, Å	1.07	C–C′–H″ bond angle, deg	121.2
C′–H″ bond dist, Å	1.07		

the binding energy and character of this orbital is the torsional motion about the C–C bond. As the CH_2 group twists, the conjugation of the 2p orbital on the terminal carbon with the C=O π bond is broken and the electrons in the 2π orbital become more localized on the CH_2 carbon atom and less tightly bound; subsequently, the 2p orbital increases in size and the electrons in it achieve relatively lower average kinetic energy.

Electronic and Vibrational Wave Functions and Energies

For our self-consistent field (SCF) calculations on the enolate anion we used an augmented standard Dunning–Huzinaga double-ζ contracted Gaussian basis set[4] labeled (9s5p/4s2p) for carbon and oxygen and (4s/2s) for hydrogen. We added diffuse p functions with exponents of 0.034 and 0.011 to each of the carbon atoms and of 0.059 to the oxygen. A full ($3N - 6 = 12$ dimensional) optimization of the equilibrium geometry of the enolate was performed; the results are reported in Table I.

To generate the neutral $HCOCH_2$ energy curve as a function of torsion angle, we performed, at each geometry for which the enolate's energy is calculated, a separate SCF calculation on the neutral. The resultant ΔSCF energy difference is well-known to underestimate the anion neutral energy gap; the anion almost always has a larger (often by as much as ca. 0.5 eV) correlation energy than the neutral. We therefore shifted the entire neutral potential energy curve relative to the anion to allow the anion and neutral curves to more accurately reproduce the known vertical detachment energy and to simulate the very close approach of the two surfaces near the perpendicular geometry.

As large amplitude distortion along the CH_2 torsion was examined, only the pyramidal "pucker" of the CH_2 group was energy optimized as a function of the torsional angle; all other bond lengths and angles were frozen. In this way, we generated an approximate "adiabatic" vibrational potential energy curve for the enolate species as a function of CH_2 torsion angle. A similar procedure was followed for the neutral radical. The one-dimensional vibrational wave functions and energies were found by numerically integrating the vibrational Schrödinger equation with an effective mass determined by the conventional[5] procedure. These adiabatic energy curves and the resulting torsional vibrational levels are shown in Figure 1.

(4) Dunning, T. H. *J. Chem. Phys.* **1970**, *53*, 2823.
(5) Wilson, E. B.; Decius, J. C.; Cross, P. C. *Molecular Vibrations*; Dover: New York, 1955.

TABLE II: State-Specific Electron Ejection Rates (10^9 s^{-1})

ν'/ν^a	9	10	11
0	3.01	5.67	3.44
1	10.9	9.13	29.5
2		34.7	17.6
3			72.5
4			6.86

[a] ν and ν' label initial- and final-state vibrational quantum numbers in the torsional mode.

TABLE III: RRKM Averaged Effective Electron Ejection Rates (10^5 s^{-1})

ν'/ν^a	9	10	11
0	6.26	3.56	0.553
1	22.7	5.73	4.74
2		21.8	2.83
3			11.7
4			1.10

[a] ν and ν' label the initial- and final-state vibrational quantum numbers in the torsional mode.

Evaluation of the nonadiabatic rate as in eq 4 requires that we compute the derivatives of the anion's electronic wave function with respect to the torsion angle $d\Psi^-/d\theta$. In doing so, we needed to evaluate, analytically, the derivatives of the Gaussian atomic basis functions with respect to θ and as well as the derivatives of the molecular orbital LCAO-MO expansion coefficients $dC_{ia}/d\theta$. The spacing between the anion and neutral vibrational levels dictates the kinetic energy of the ejected electron and hence the value of k which enters into the free-electron wave function ϕ_k.

Discussion of Results of Simulations of Ejected Rates

Our calculated *state-specific* rates of electron ejection shown in Table II vary from 10^9 s^{-1} to nearly 10^{11} s^{-1}. Unfortunately, our state-specific rates on $HCOCH_2^-$ are difficult to compare directly with the experimental data on $H_3CCOCH_2^-$. The experiments do *not* prepare the anions in only one internal quantum state. At best, one can use the laser fluence and pulse duration together with an estimate of the IR absorption cross section of the ion to estimate the *average* number of photons the ions have absorbed. However, this energy is certainly not concentrated in the CH_2 torsional mode. Therefore, to simulate the experimental conditions as closely as possible (but for $HCOCH_2^-$ and not $H_3CCOCH_2^-$), we considered a situation in which enough IR photons have been absorbed to place the anion 4000 cm^{-1} above its detachment threshold. This choice of 16 500-cm^{-1} total internal energy was made simply to generate a situation in which the $9 \leq \nu \leq 11$ states of the anion can, in principle, be populated; these are the states for which we have computed electron ejection rates. However, this amount of internal energy E also represents reasonably well the experimental situation described earlier for acetone enolate—the anion with internal energy considerably above its detachment threshold. We used an RRKM model to describe how the total energy of 16 500 cm^{-1} is distributed among the internal vibrations of the enolate. For a total internal energy E, we obtain an RRKM estimate[6] of the total number ($N(E)$; see Figure 2 for a plot of $N(E)$ vs E) of states (within ± 1 cm^{-1}) for the 12 vibrational degree of freedom $HCOCH_2^-$. We then subtract from E an amount of energy $E(n)$ corresponding to the energy of the CH_2 torsional mode having n quanta of excitation. RRKM theory is then once again used to compute the number $N^*(E - E(n))$ of states (within ± 1 cm^{-1}) for the 11 remaining vibrational degrees of freedom (i.e., with the CH_2 torsion removed) at an energy $E - E(n)$. The ratio $P_n \equiv N^*(E - E(n))/N(E)$ is then taken as proportional to the probability that the torsional mode is excited to level n given a total amount of internal energy E. The *effective* decay rate for each anion vibrational state (v) is then computed

(6) For the $-CH_2$ torsional mode, we used the actual (Figure 1) vibrational energy levels. For all other modes, we used harmonic vibrational energies; the resultant RRKM total state densities are not strongly affected by this harmonic approximation at the total internal energies used in our calculations.

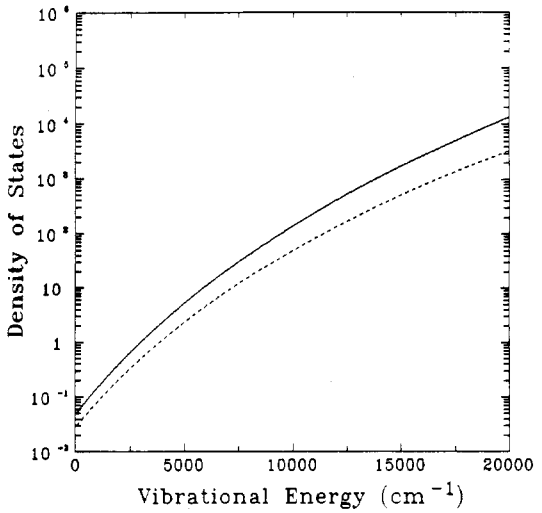

Figure 2. Density of vibrational states as a function of total vibrational energy. Solid line is for 12 vibrational degrees of freedom, dashed line is for 11 vibrational degrees of freedom.

as the probability of being in that state times the state-specific decay rate from Table II. The resultant effective decay rates are given in Table III.

Obviously, the RRKM averaged decay rates are considerably slower than the state-specific rates. This difference reflects the low occupation probabilities (10^{-4}–10^{-5}) of v = 9, 10, 11 in the anion's torsional mode at a total excitation energy corresponding to 16 500 cm^{-1}. Incredibly, the average lifetimes of the v = 9, 10, 11 anion states lie in the 10^{-6}–10^{-7}-s range inferred from the experimental data on acetone enolate. The fact that our first principles simulation generates absolute rates that are in agreement with the experimental data implies that the VIED process is indeed a plausible mechanism for the electron loss seen in numerous IR-photon excited anions.

As pointed out in the following paper by the Brauman group,[3] the frequency of passage ν_p over or near the torsional barrier, which can be evaluated in terms of the oscillation frequency ($\sim 4.5 \times 10^{13}$ s^{-1}) of the torsional mode multiplied by the probability P of being in a state (v = 9, 10, 11) that samples this region ($P \sim 10^{-4}$–10^{-5}), is approximately $\nu_p \sim 4 \times 10^8$–4×10^9 s^{-1}. The fact that electrons are ejected only at a rate of $\sim 10^7$ s^{-1} means that only 1/400 – 1/40 of the torsional passages over or near the barrier result in ejection. In other words, if vibration-to-electronic energy flow were extremely facile, electron ejection could occur at rates in the 10^8–10^9-s^{-1} range as determined by Franck–Condon-like factors and torsional oscillation frequencies. When proper account is made of nonadiabatic vibration-to-electronic energy flow, these limiting rates are reduced by factors of 10^{-4}–10^{-5}.

Summary

We used ab initio electronic structure methods within a perturbative (Fermi Golden Rule) treatment of non-Born–Oppenheimer couplings to compute the state-specific rates of electron loss for excited torsional vibrational states of $HCOCH_2^-$. These state-to-state rates were found to range from 3×10^9 to 7×10^{10} s^{-1}. Combining these rates with an RRKM model for partitioning 16 500 cm^{-1} of internal vibrational energy among the modes of $HCOCH_2^-$, we arrive at an *effective* or average rate of electron loss for $HCOCH_2^-$ of 10^7 s^{-1}, which agrees remarkably well with the rate inferred from experimental data on $H_3CCOCH_2^-$, thereby supporting the non-Born–Oppenheimer process as the cause of electron loss.

Acknowledgment. We acknowledge the financial support of the National Science Foundation (CHE-8511307). Some calculations associated with this work were done at the San Diego Supercomputer Center.

Vibrationally Induced Electron Detachment. A Rate for Electron Loss from Vibrationally Excited Acetone Enolate Anion

Robert F. Foster,† William Tumas,‡ and John I. Brauman*

Department of Chemistry, Stanford University, Stanford, California 94305-5080 *(Received: June 24, 1988)*

A rate for electron autodetachment from vibrationally excited acetone enolate anion in the gas phase has been deduced experimentally from the observation of photochemical branching between an adiabatic fragmentation channel and a nonadiabatic vibrationally induced electron detachment channel under collisionless conditions using ion cyclotron resonance spectrometry. Infrared multiple-photon activation of acetone enolate anion with a pulsed CO_2 laser results in both methane elimination to produce deprotonated ketene anion and electron detachment. These results coupled with thermochemical and mechanistic considerations as well as statistical reaction rate theory calculations lead to an estimated rate for electron autodetachment from the vibrationally excited anion of 10^7 s^{-1} at an energy ca. 1 eV above threshold. The experimental details as well as the calculations and modeling involved in this determination are presented along with an evaluation of proposed models for vibrational-to-electronic coupling.

Introduction and Background

Highly vibrationally excited molecules often exhibit unique properties and reactivities. Since the energy required to remove an electron from a negative ion (i.e., the electron affinity (EA) of the corresponding radical) is often much less than the energy necessary to break chemical bonds, gas-phase anions offer the interesting possibility of decomposition by loss of an electron upon IR laser activation. Vibrationally induced electron detachment (VED) was first demonstrated by Rosenfeld et al.[1] in studies on the IR laser photochemistry of benzyl anion using ion cyclotron resonance (ICR) spectrometry. Electron loss was the only observed photoprocess in benzyl anion irradiated with a pulsed CO_2 laser under collisionless conditions. Subsequently, Wight and Beauchamp[2] reported that this reaction could be induced via low-power continuous wave CO_2 laser irradiation as well.

$$PhCH_2^- \rightarrow PhCH_2^{\bullet} + e^- \quad (1)$$

† Drytek, Wilmington, MA 01887.
‡ Central Research and Development, E. I. du Pont de Nemours and Co., Experimental Station, Wilmington, DE 19898.

(1) Rosenfeld, R. N.; Jasinski, J. M.; Brauman, J. I. *J. Chem. Phys.* **1979**, *71*, 1030.
(2) Wight, C. A.; Beauchamp, J. L. *J. Am. Chem. Soc.* **1981**, *103*, 6499.

0022-3654/89/2093-0061$01.50/0